Effects of Slow Substrate Binding and Release in Redox Enzymes: Theory and Application to Periplasmic Nitrate Reductase

Patrick Bertrand,[†] Bettina Frangioni,[†] Sébastien Dementin,[†,‡] Monique Sabaty,[‡] Pascal Arnoux,[‡] Bruno Guigliarelli,[†] David Pignol,[‡] and Christophe Léger*,[†]

Laboratoire de Bioénergétique et Ingénierie des Protéines, CNRS UPR 9036, IBSM, and Université de Provence, 31 chemin Joseph Aiguier, 13009 Marseille, France, and Laboratoire de Bioénergétique Cellulaire, iBEB, UMR 6191, CEA/CNRS, and Université Aix-Marseille II, CEA Cadarache, 13108 Saint Paul lez Durance, France

Received: June 5, 2007

For redox enzymes, the technique called protein film voltammetry makes it possible to determine the entire profile of activity against driving force by having the enzyme exchanging directly electrons with the rotating-disc electrode onto which it is adsorbed. Both the potential location of the catalytic response and its detailed shape report on the sequence of catalytic events, electron transfers and chemical steps, but the models that have been used so far to decipher this signal lack generality. For example, it was often proposed that substrate binding to multiple redox states of the active site may explain that turnover is greater in a certain window of electrode potential, but no fully analytical treatment has been given. Here, we derive (i) the general current equation for the case of reversible substrate binding to any redox states of a two-electron active site (as exemplified by flavins and Mo cofactors), (ii) the quantitative conditions for an extremum in activity to occur, and (iii) the expressions from which the substrate-concentration dependence of the catalytic potential can be interpreted to learn about the kinetics of substrate binding and how this affects the reduction potential of the active site. Not only does slow substrate binding and release make the catalytic wave shape highly complex, but we also show that it can have important consequences which will escape detection in traditional experiments: the position of the wave (this is the driving force that is required to elicit catalysis) departs from the reduction potential of the active site even at the lowest substrate concentration, and this deviation may be large if substrate binding is irreversible. This occurs in the reductive half-cycle of periplasmic nitrate reductase where irreversibility lowers the driving force required to reduce the active site under turnover conditions and favors intramolecular electron transfer from the proximal $[4Fe4S]^{+}$ cluster to the active site Mo^{V}.

Introduction

Protein film voltammetry (PFV) is an electrochemical technique where the enzyme is adsorbed onto an electrode surface and electron transfer is direct.[1,2] In such a configuration, in the presence of substrate and provided the electrode is rotated at high speed to avoid mass transport limitations, the entire profile of steady-state activity (current, *i*) against driving force (electrode potential, *E*) is recorded in the form of a catalytic voltammogram (or "wave") whose shape can be complex and often embeds a wealth of information about the catalytic mechanism. Deciphering the electrochemical response in relation to the catalytic mechanism[3] is a challenge which we contribute to tackle.

The electrode potential where the activity kicks on (defined as the inflection point of the "main" sigmoidal transition toward the first plateau or peak) is an important characteristics of the steady-state current response because this relates to the minimal driving force that must be provided by the physiological redox partner of the enzyme.[4] This catalytic, or "operating", potential is somehow related to the reduction potential of the active site, since substrate transformation can proceed only when the active site converts into a certain redox state (usually fully reduced or oxidized). The catalytic potential is also affected by the kinetics of intramolecular electron transfer (ET) on condition that this process partly limits the turnover rate,[5] and most obviously by substrate binding (including protonations).[6,7] All of these effects are potentially important in making the redox properties match catalytic function.[8]

At high overpotential, the catalytic wave often shows one or two other sigmoidal features. For example, the activity may be "boosted" when a certain electrode potential is reached.[9−11] Instead, it may be attenuated or even "switched off" as the driving force is increased. The observation that the turnover rate of a redox enzyme may not merely increase in a monotonic fashion upon increasing the driving force was first made in an early study of fumarate reduction by mitochondrial complex II.[12,13] It was proposed that the existence of a window of electrode potential where the reductive activity is optimized results from the fact that fumarate binds to the active site flavin only when the latter is oxidized, whereas the flavin needs to be reduced for catalysis to occur; according to this hypothesis, the attenuation of activity at high driving force results from the low affinity for the substrate of the redox state of the active site that is competent to turn it over.[12]

A more complex mechanism involving differential binding of substrate to any redox state of the active site was suggested

* Corresponding author. E-mail: christophe.leger@ibsm.cnrs-mrs.fr.
[†] CNRS Marseille.
[‡] CEA Cadarache.

10.1021/jp074340j CCC: $37.00
Published on Web 08/04/2007

as a general explanation of the complex voltammetric wave shapes observed for adsorbed enzymes,[4] but no quantitative analysis was attempted. In fact, most available electrochemical models for adsorbed enzymes assume that substrate binds only when the active site is in the redox state that is competent to transform it,[3,14−17] with the immediate consequence that only simple (sigmoidal) wave shapes are predicted. Hirst et al.[15] and Butt et al.[18] did use a kinetic scheme based on the assumption that substrate binds to two redox states of the active site rather than one, but this greatly increases the number of parameters and the current equations were not factorized into expressions that can be easily discussed or used to fit the data. In a previous communication, we were able to derive a simple rate equation using the assumption that substrate binding to two redox states of the active site is fully irreversible on the time scale of turnover.[19] Alternatively, the results are often analyzed at an empirical level, with current equations designed *ad hoc* by combining sigmoidal functions,[20−25] in which case the adjusted parameters, including the catalytic and switch potentials, have no explicit physical meanings.

In the first part of this paper, we shall examine in detail how the thermodynamics and kinetics of substrate binding affects the position and shape of a catalytic voltammogram in the most general case where substrate can bind to and be released from any redox state of the active site. We shall make no assumption regarding the rate of this process, and binding to a single redox state will be regarded as a peculiar case. General conclusions will be drawn regarding how substrate binding affects the position of the main catalytic wave and the overall shape of the signal and, conversely, how the substrate-concentration dependence of the catalytic potential can be interpreted to learn about the thermodynamics and kinetics of substrate binding in the catalytic cycle.

In the subsequent, experimental section, we apply this model to the peculiar case of *Rhodobacter sphaeroides* periplasmic nitrate reductase (NapAB), whose structure we recently determined.[26] It belongs to the so-called "DMSO reductase family" of mononuclear molybdoenzymes, which collects bacterial enzymes of diverse functions despite housing similar active sites.[27] These enzymes specifically transform small inorganic compounds such as nitrate and dimethyl sulfoxide (DMSO), often in an oxo-transfer reaction coupled to the transfer of two electrons and two protons. They intervene in the global carbon, sulfur, and nitrogen cycles, and some of their substrates, including arsenite and selenate, are toxic anions whose abundance in both natural and humanly impacted environments is an important issue of current public health. All members of the DMSO reductase family contain a conserved catalytic subunit where the active site Mo is bound to two pterin molecules, resulting in a minimal coordination of the metal by four thiolates. These enzymes are remarkably diverse in terms of oligomeric architecture and cofactor content. Accessory modules may be connected to the catalytic subunit to provide the electron-transfer chain and, in some cases, the site of interaction with the quinone pool.[28−30] An iron−sulfur (FeS) cluster proximal to the Mo cofactor (Moco) is always present in the catalytic subunit of multicenter enzymes; this cluster is a [4Fe4S] cluster in all cases but arsenite oxidases, where electrons are transferred from the active site to a high potential [3Fe4S] cluster.[31] Also unique to arsenite oxidases is the fact that the Moco is not covalently attached to the protein. NapAB is a water-soluble, tight complex that consists of a large catalytic subunit (NapA; 91 kDa), containing a [4Fe4S] cluster and the molybdenum active site cofactor (Moco), and of a small electron transfer (ET) subunit

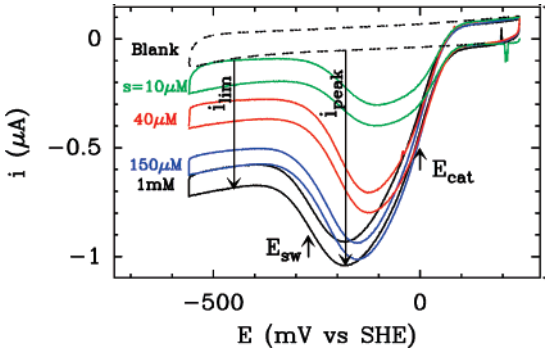

Figure 1. Activity against electrode potential for NapAB adsorbed onto a graphite electrode. The more negative the current, the greater the activity. E_{cat} and E_{sw} are the inflection points of the voltammograms. The nitrate concentration, s, is indicated on the left of each signal, pH 8, $T = 20$ °C, electrode rotation rate $\omega = 2$ krpm, electrode-potential scan rate $\nu = 50$ mV/s.

(NapB; 17 kDa), housing two surface-exposed *c*-type hemes. It catalyzes the first step in denitrification under both aerobic and anaerobic conditions, and *in vitro*, it is also able to reduce chlorate, selenate, and tellurite.[32]

Figure 1 shows steady-state voltammograms for nitrate reduction by NapAB adsorbed onto a pyrolytic graphite edge (PGE) rotating-disc electrode.[19] When the electrode potential is taken to more negative values, the activity first increases to a maximum (*i* decreases to a minimum) before it drops and eventually plateaus off at high driving force. The electrochemical signature of NapAB in Figure 1 is similar for all other enzymes from the DMSO reductase family for which PFV data are available[4,18,25,33,34] with the exception of arsenite oxidases.[35,36] As mentioned above, these enzymes share a common catalytic subunit but they have very little overall homology, suggesting that the electrochemical data relate to the mechanism at the active site. We shall use the theoretical model we propose to discuss the position of the wave, to discuss the reason the maximal reductase activity is not obtained under the most reducing conditions, and to fit the data over a range of experimental conditions that is large enough to enable the determination of the succession of chemical events (substrate binding, protonations) that are coupled to the reduction of the active site under turnover conditions. We emphasize the consequences of the mechanism we propose on the thermodynamics of intramolecular ET, and we explain why this is likely to apply to other reductases from the DMSO reductase family.

Experimental Procedures

Protein samples were prepared as described in ref 26.

We used the same electrochemical setup and equipment as described in ref 37. The enzyme was adsorbed onto a pyrolytic graphite edge electrode by painting the surface with about 0.5 μL of stock solution of enzyme (≈100 μM in 20 mM *N*-(2-hydroxyethyl)piperazine-*N*′-ethanesulfonic acid (HEPES), 0.1 M NaCl pH 7.5) after it had been coated with 200 mM neomycin sulfate in water (SIGMA. *Caution: May be harmful if inhaled or swallowed, or if absorbed through the skin. Skin, eye, and respiratory irritant. May cause allergic reaction or sensitization.*); this was found to increase the stability of the film. Stock solutions of potassium nitrate (PROLABO. *Caution: Harmful if swallowed. Skin, eye, and respiratory irritant.*), sodium nitrite (SIGMA. *Caution: Toxic if swallowed. Severe eye irritant. Respiratory and skin irritant. May act as a carcinogen for chronic exposure. Very toxic to aquatic organisms.*), or sodium azide (PROLABO. *Caution: Mutagen, harmful by inhalation,*

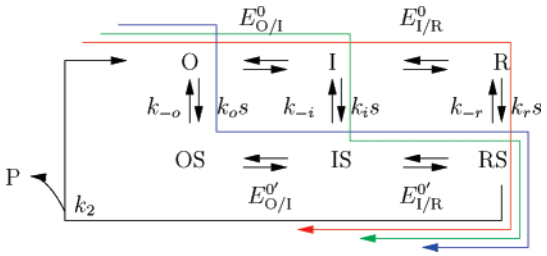

Figure 2. Catalytic schemes for interpreting the voltammetry. The horizontal arrows are for redox transitions, while the vertical arrows depict chemical transformations, including reversible substrate (S) binding and irreversible product (P) formation and release. This leads to the current eq 2. The red arrow is the catalytic pathway that is necessarily taken at low electrode potential; the green and blue arrows are alternative pathways which may be operational at moderate driving force.

ingestion, or skin contact. Ingestion or inhalation may be fatal. Material is readily absorbed through skin. Very toxic in the environment.) were added to the cell to give the desired final concentrations. The mixed buffer consisted of 2-morpholinoethanesulfonate (MES), *N*-[2-hydroxyethyl]piperazine-*N*′-[2-ethanesulfonic acid] (HEPES), sodium acetate, *N*-tris[hydroxymethyl]methyl-3-aminopropanesulfonic acid (TAPS), and CHES (all from SIGMA, each component had a concentration of 5 mM). The data were analyzed using the in-house program "SOAS", which embeds regression[38] and Fourier transform routines available on the NETLIB repository.

Electron paramagnetic resonance (EPR) experiments were performed on a Bruker ELEXSYS 500E spectrometer fitted with an Oxford Instrument ESR900 helium flow cryostat. Potentiometric titrations were performed in an anaerobic cell flushed with argon. A cocktail of mediators was added to the protein solution to accelerate the redox equilibration. Samples were poised at various potentials by adding small volumes of sodium dithionite (10 mM in water), then quickly and anaerobically frozen in liquid nitrogen. The buffer was 16 mM HEPES, 15 mM tris(hydroxymethyl)aminomethane (Tris), and 65 mM NaCl at pH 7.2 or 110 mM tricine, 5 mM HEPES, and 65 mM NaCl at pH 9.1.

The General Model

Phenomenological Parameters. Following common practice,[20−25,39] we term E_{cat} and E_{sw} (after "catalysis" and "switch") the potentials of the high and low potential inflection points of the voltammograms, respectively, and i_{peak} and i_{lim} the maximal and limiting currents (see Figure 1). It is also useful to quantify the steepness of the features of the catalytic voltammograms by the nondimensional parameters n_{cat} and n_{sw}, obtained by fitting the different portions of the catalytic signal to sigmoidal functions, for example,

$$i \propto \frac{-1}{1+\exp[n_{cat}\, f(E-E_{cat})]} \tag{1}$$

for the low driving force (high potential) part. We note $f = F/RT$. Typical "*n* values" are in the range 1−2; the greater the n_{cat} value, the steeper the sigmoid. Our rigorous analysis below gives these parameters physical meaning.

The Rate Equation. We interpret the kinetics on the basis of the six-member scheme in Figure 2.[25] We consider the three redox states of the active site, O (oxidized), I (intermediate, or half-reduced), and R (reduced). These may correspond to the quinone, semiquinone, and hydroquinone forms of active site flavins or to the Moco in its redox states VI, V, and IV, respectively. We depict as horizontal arrows the redox transformations between these states and we note $E^\circ_{O/I}$ and $E^\circ_{I/R}$ as their reduction potentials. The vertical steps correspond to substrate binding with pseudo-first-order rate constants $k_o s$, $k_i s$, and $k_r s$ (s is the substrate concentration) and substrate release with first-order rate constants k_{-o}, k_{-i}, and k_{-r}. The substrate-bound, reduced active site (RS) is transformed into O with the first-order rate constant k_2 which incorporates substrate transformation and product release; it is common practice to group into a single transformation a series of steps whose rates cannot be influenced by the experimental parameters (doing otherwise only adds parameters that cannot be independently determined).[40] The reduction potential of the substrate-bound OS/IS couple is defined by $E^{\circ\prime}_{O/I} = E^\circ_{O/I} + f^{-1}\ln(K_o/K_i)$, where $K_o = k_{-o}/k_o$ and K_i are the dissociation constants. A similar relation holds for $E^{\circ\prime}_{I/R}$. In this paper, only the case of reductive catalysis is addressed; all equations for the oxidative process can be straightforwardly obtained from those we give by swapping subscripts r and o and changing F into $-F$. A complete list of symbols is given in the Supporting Information.

The derivation of the rate equation is greatly simplified by making the following hypotheses:

(i) Catalysis is at steady state. In experiments carried out at small scan rate, the validity of this assumption will easily be assessed by checking that the catalytic current is independent of scan rate or scan direction.

(ii) Both interfacial and intramolecular ET steps are fast with respect to turnover, so that the catalytic intermediates are in redox equilibrium in the steady state, and their concentrations are given by Nernst equations.[5,7] The assumption that interfacial ET is fast will prove valid in the case of NapAB. In other situations, the catalytic signal may be broadened by slow electron transfer at the enzyme/electrode interface, but from an operational perspective, this does not preclude the measurement of the catalytic potential, whose value will be interpreted with the model we provide.[5,7]

(iii) There is neither inhibition by nor back-reaction with the product. This assumption will be proved accurate in our study of NapAB, but it may not apply in some particular cases.[7] However, we note that product inhibition is usually taken into account only when the product accumulates during the experiment.[40] Using a rotating electrode, it is spun away from the adsorbed enzyme and its concentration should remain very small.

(iv) There is no substrate depletion near the electrode surface, despite substrate being consumed by the adsorbed enzyme. That this is true for a certain electrode rotation rate, ω, is proved in experiments by the fact that increasing ω further produces no increase in current.

As demonstrated in the Supporting Information, the activity increases from naught at high electrode potential to a limiting value, i_{lim}, at high driving force according to

$$i_{lim} = -\frac{2FA\Gamma k_2}{1+K_m^{lim}/s} \tag{2a}$$

$$K_m^{lim} = \frac{k_2+k_{-r}}{k_r} = K_r\left(1+\frac{k_2}{k_{-r}}\right) \tag{2b}$$

$$i = g(E, s, A\Gamma, E^\circ_{O/I}, E^\circ_{I/R}, k_2, k_o, K_o, k_i, K_i, k_r, K_r) \tag{2c}$$

K_m^{lim} is the Michaelis constant at high driving force (on the plateau). We note A as the electrode surface and Γ as the electroactive coverage of enzyme. Equation 2a demonstrates that

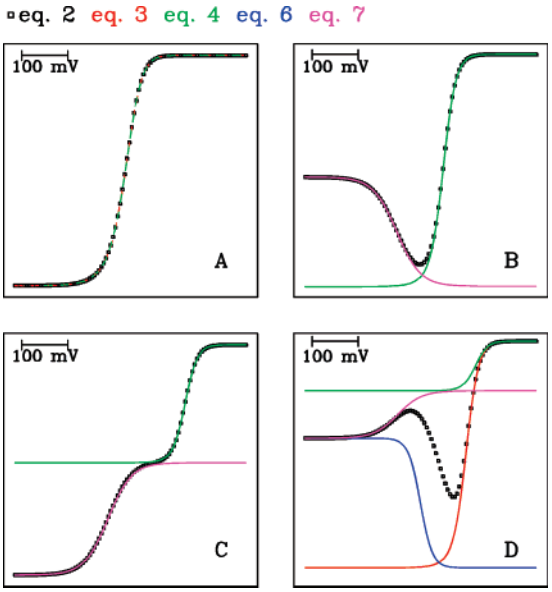

Figure 3. Examples of catalytic voltammograms calculated from eq 2 (black squares) and approximations given by eqs 3 (red line), 4 (green line), 6 (blue line), and 7 (purple line). The parameters that were used to calculate these curves are given in the Supporting information. In panel A, the green and red curves overlay because $\alpha_i = \alpha_o = 1$. In each plot, the horizontal segment marks $i = 0$ and has a width of 100 mV, $T = 25$ °C.

the limiting current follows Michaelis−Menten kinetics even though substrate can bind to all three redox states of the active site. At high driving force and under saturating conditions, the activity tends to a value that is proportional to k_2; this may be faster than the turnover number measured in solution assays, since the latter incorporates the rate of reduction of the enzyme by the redox partner, whereas this process is assumed to be infinitely fast in the low potential limit. As is the case in homogeneous kinetics,[40] the limiting Michaelis constant in eq 2b equates the true dissociation constant, K_r, only if catalysis is slow with respect to substrate release from R ($k_2 \ll k_{-r}$). However, the Michaelis constant measured in solution assays potentially depends on all rates in the catalytic cycle, including those for the reductive half-cycle, and will therefore depart from K_m^{lim} if intermolecular ET is rate determining in solution assays.

From eqs 2a and b, it is clear that the magnitude of the low potential current may be used to determine K_m^{lim} and k_2 (provided the electroactive coverage, $A\Gamma$, is known) but that it contains little information about the catalytic cycle. In contrast, we demonstrate below that the shape and position of the catalytic signal, and their dependence on substrate concentration and pH, can be used to determine the entire sequence of events which define the catalytic reductive half-cycle, and the thermodynamic properties (reduction potentials and dissociation constants) of some of the intermediates.

The function g gives the dependence of i on the experimental parameters s, E, and $A\Gamma$ and on the nine independent parameters in the scheme of Figure 2; it is given in the Supporting Information (eq S3), where we use the notation $\alpha_i = k_i/k_r$ and $\alpha_o = k_o/k_r$. Figure 3 illustrates the variety of wave shapes that can be calculated from eq 2, all of which have already been observed in various contexts.[1,34,41] Depending on the values of the parameters, each feature can be best fit to a sigmoidal function with an apparent number of electrons ranging from one to two, although each portion of these waves need not be exactly sigmoidal. Since differentiating eq 2c did not lead to *simple* expressions for the coordinates of the inflection points, we derived approximate expressions for the low and high driving force parts of the wave (solid lines in Figure 3), from which the positions of the main features can be predicted. The price to pay for this simplification is that there is not a single pair of functions that can be used to describe the low and high potential limits of the wave, and one shall consider distinct approximations according to whether the half-reduced state of the active site is thermodynamically stable or unstable.

The Main Wave and the Meaning of E_{cat}. We obtained eq 3 from eq 2 by taking the limit where the electrode potential is high. This equation describes accurately the low driving force part of the wave, and we found that it often also approximates very well the *entire* wave shape when the latter is close to having only one inflection point (i.e., when the wave has no switch nor "boost"; see, for example, Figure 3A).

$$i \approx \frac{i'}{1 + \exp[f(E - E_{cat}^{n=1})] + \exp[2f(E - E_{cat}^{n=2})]} \quad (3a)$$

$$i' = -\frac{2FA\Gamma k_2}{1 + K'/s} \quad (3b)$$

$$K' = \frac{K_m^{lim} + (\alpha_o - 1)K_r}{\alpha_o} = K_r\left(1 + \frac{k_2}{\alpha_o k_{-r}}\right) \quad (3c)$$

$$E_{cat}^{n=1} = \underbrace{E_{I/R}^{\circ} + \frac{1}{f}\ln\frac{K_i}{K_r}}_{E_{I/R}^{\circ\prime}} + \frac{1}{f}\ln\frac{s + K'}{s + K_i} \quad (3d)$$

$$E_{cat}^{n=2} = \underbrace{E_{O/R}^{\circ} + \frac{1}{2f}\ln\frac{K_o}{K_r}}_{E_{O/R}^{\circ\prime}} + \frac{1}{2f}\ln\frac{s + K'}{s + K_o} \quad (3e)$$

The wave predicted by eq 3 is either "one-" or "two-electron", or may broaden from $n = 2$ to $n = 1$ as the driving force increases. Although eq 3a is not that of a sigmoid, in practice, it will tend and fit very well to eq 1 with $n_{cat} = 1$ and $E_{cat} = E_{cat}^{n=1}$ if $E_{cat}^{n=1} \ll E_{cat}^{n=2}$ or with $n_{cat} = 2$ and $E_{cat} = E_{cat}^{n=2}$ if $E_{cat}^{n=1} \gg E_{cat}^{n=2}$.

The $n = 1$ wave is more likely to be observed if the half-reduced state of the active site is thermodynamically stable (i.e., when $\delta = \exp[f(E_{I/R}^{\circ} - E_{O/I}^{\circ})]$ is small). However, in that situation, we demonstrate in the Supporting Information that a more accurate and meaningful approximation reads

$$i \approx \frac{i'}{1 + \exp[f(E - E_{cat}^{n=1})] + \exp[2f(E - E_{cat}^{n=2})]} \quad (4a)$$

$$i' = -\frac{2FA\Gamma k_2}{1 + K'/s} \quad (4b)$$

$$K' = \frac{K_m^{lim} + (\alpha_i - 1)K_r}{\alpha_i} = K_r\left(1 + \frac{k_2}{\alpha_i k_{-r}}\right) \quad (4c)$$

$$E_{cat}^{n=1} = E_{I/R}^{\circ} + \frac{1}{f}\ln\frac{K_i}{K_r} + \frac{1}{f}\ln\frac{s + K'}{s + K_i} \quad (4d)$$

$$E_{cat}^{n=2} = E_{O/R}^{\circ} + \frac{1}{2f}\ln\frac{K_o}{K_r} + \frac{1}{2f}\ln\frac{s + K'}{s + K_o} \quad (4e)$$

Note that α_i now substitutes for α_o in the expression of K'.

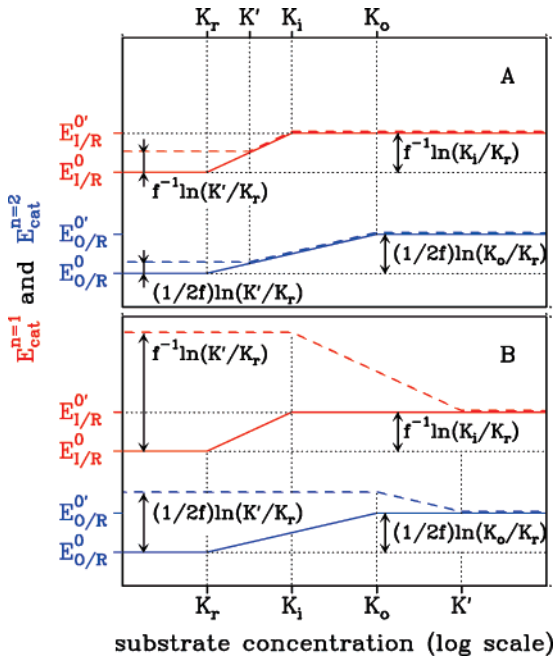

Figure 4. Pourbaix-like diagrams showing the concentration dependences of $E_{cat}^{n=1}$ (red) and $E_{cat}^{n=2}$ (blue); s increases from left to right on a logarithmic scale. We chose $\alpha_i = \alpha_o = 1$ (so that eqs 3 and 4 are identical and $K_m^{lim} = K'$) and $K_r < K_i < K_o$. The dashed lines show the behaviors predicted by eq 3d/4d and eq 3e; the continuous red line shows the limit given by eq 5 which is valid when k_2 is infinitely small. Panel A illustrates the case where k_2 is small enough that K' is only slightly greater than K_r. Panel B illustrates the case $K_r \ll K'$.

Hence, the inflection points of a two- or one-electron wave may be interpreted using eq 3e or 4d, respectively. In the following, we discuss several limiting situations regarding the interpretation of $E_{cat}^{n=1}$; the reasoning is similar for the position of the two-electron wave.

When substrate transformation is slow (strictly, when $k_2 \ll k_{-r}$ and $k_2 \ll \alpha_i k_{-r}$), both K_m^{lim} and K' tend to K_r (cf. eqs 2b and 4c); in this limit where substrate binding is at equilibrium in the steady state, eq 4d reads

$$E_{cat}^{n=1} = E_{I/R}^{\circ} + \frac{1}{f}\ln\frac{1 + s/K_r}{1 + s/K_i} \tag{5}$$

as illustrated by the continuous red lines in Figure 4. This relation was already obtained and used in relation to the voltammograms for succinate oxidation by adsorbed *E. coli* fumarate reductase (see the discussion of eq 4 in ref 6).

In the general case, $E_{cat}^{n=1}$ tends to $E_{I/R}^{\circ\prime}$ (the reduction potential of the I/R couple when the active site is bound to substrate) when s is larger than both K' and K_i. Remarkably, at low substrate concentration, the position of the one-electron wave tends to a limit which departs from the reduction potential of the substrate-free active site (dashed red lines in Figure 4). Even when s is lower than both K' and K_i, $E_{cat}^{n=1}$ remains shifted from $E_{I/R}^{\circ}$ by an amount of $f^{-1}\ln[1 + K'/K_r] = f^{-1}\ln[1 + k_2/(\alpha_i k_{-r})]$ which tends to zero only if substrate release is very fast.

This has an important consequence regarding the qualitative interpretation of the position of a catalytic wave for an adsorbed enzyme: even at the lowest substrate concentrations, the value of E_{cat} cannot be straightforwardly interpreted as the reduction potential of the substrate-free active site.

The Switch. We found that either of two simple functions accurately matches the high driving force part of the voltammogram. The choice of which function is more appropriate depends on whether the data are best described by a one- or two-electron sigmoid.

The situation where the high driving force feature of the voltammogram is sharp ($n = 2$, as is the case for mitochondrial complex II[12,20−22]) is more likely to occur when the half-reduced state of the active site is thermodynamically unstable (i.e., when $\delta = \exp[f(E_{I/R}^{\circ} - E_{O/I}^{\circ})]$ is large), in which case the right approximation is

$$\frac{i}{i_{lim}} \approx 1 + \frac{-K_r s + K_o[(\alpha_o - 1)K_m^{lim} - \alpha_o K_r]}{K_o(s + K_m^{lim})} \times \frac{\exp[2f(E - E_{O/R}^{\circ})]}{1 + \exp[2f(E - E_{sw}^{n=2})]} \tag{6a}$$

$$E_{sw}^{n=2} = E_{O/R}^{\circ} + \frac{1}{2f}\ln\frac{K_o}{K_r + \alpha_o K_o} + \frac{1}{2f}\ln\frac{s + K_m^{lim}}{s + K_o\dfrac{K_m^{lim} + \alpha_o K_r}{K_r + \alpha_o K_o}} \tag{6b}$$

Otherwise, if the high driving force feature of the wave looks like an $n = 1$ sigmoid,

$$\frac{i}{i_{lim}} \approx 1 + \frac{-K_r s + K_i[(\alpha_i - 1)K_m^{lim} - \alpha_i K_r]}{K_i(s + K_m^{lim})} \times \frac{\exp[f(E - E_{I/R}^{\circ})]}{1 + \exp[f(E - E_{sw}^{n=1})]} \tag{7a}$$

$$E_{sw}^{n=1} = E_{I/R}^{\circ} + \frac{1}{f}\ln\frac{K_i}{K_r + \alpha_i K_i} + \frac{1}{f}\ln\frac{s + K_m^{lim}}{s + K_i\dfrac{K_m^{lim} + \alpha_i K_r}{K_r + \alpha_i K_i}} \tag{7b}$$

Analyzing the sign of the first fraction in eq 7a leads to a necessary (but not sufficient) condition for an $n = 1$ switch to exist:

$$\alpha_i = k_i/k_r > \alpha_i^{min} \tag{8a}$$

$$\alpha_i^{min} = 1 + \frac{K_r}{K_i}\frac{s + K_i}{K_m^{lim} - K_r} \tag{8b}$$

An equation similar to eq 8 can be derived from eq 6a for the two-electron switch. From eq 8, we conclude that there can be no one-electron switch unless $\alpha_i > 1$. For a given value of α_i, the parameters that decrease α_i^{min} favor an $n = 1$ switch: these are (i) irreversibility of substrate binding on the time scale of turnover (this increases the difference between K_m^{lim} and K_r; see eq 2b), and (ii) a low concentration of substrate. Equation 8 predicts that the switch should disappear when s exceeds a certain value: this is a consequence in our model of the rates of binding being proportional to s and increasing as s is raised until the step whose rate is k_2 fully limits turnover. However, we note that the substrate concentration that makes α_i^{min} greater than α_i (and the switch disappear) is not simply related to, and can be much greater than, K_m^{lim}.

Experimental Results

Direct Electrochemistry versus Solution Assays. Figure 1 shows voltammograms for nitrate reduction by NapAB adsorbed

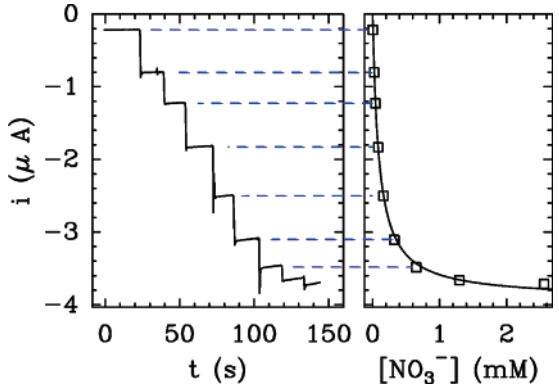

Figure 5. Chronoamperometric determination of the Michaelis constant for nitrate reduction. The electrode was poised at −450 mV vs SHE, rotated at 2 krpm, and nitrate was added from stock solutions while the activity was continuously recorded as a current. In the right panel, the change in current is fit to the Michaelis−Menten equation with $K_m^{lim} = 95\ \mu$M. pH 7, $T = 20$ °C.

onto a rotating pyrolytic graphite edge (PGE) electrode. Since no direct (noncatalyzed) nitrate reduction occurs on graphite,[34,42] the current is simply proportional to the rate of catalytic nitrate reduction (the more negative the current, the greater the turnover number). The experiments have been performed with the same NapAB film successively transferred to pH-buffered solutions of increasing nitrate concentration in the range $s = 10\ \mu$M to 1 mM. Upon lowering the electrode potential, E, the activity reaches a maximum before leveling off at high driving force, and the same variation in activity is observed on the subsequent scan toward high E, showing that kinetics occurs at (or at least close to) steady state.

The electrode rotation rate was high enough that increasing it further produced no significant increase in current; thus, there was neither substrate depletion near the electrode surface nor inhibition by the product nitrite,[7] and consistently, adding a large amount of nitrite to the buffer while the enzyme reduces nitrate does not decrease the catalytic current (we checked this by adding 300 μM nitrite to a solution containing 20 μM nitrate).

Measuring the turnover number from catalytic voltammograms requires that the electroactive coverage be known.[1,6,43] The latter can only be measured from the magnitude of the current recorded in the absence of substrate, which reveals the stoichiometric oxidation/reduction of all the redox centers in the adsorbed enzyme. In the case of NapAB, however, and as often occurs, we could not detect reliable noncatalytic signals, and this precluded us from determining the electroactive coverage and the turnover number of the adsorbed enzyme. However, the Michaelis constant can be measured from the change in limiting current against substrate concentration even if the electroactive coverage is unknown, provided it is constant. The left panel in Figure 5 shows the change in current against time in an experiment where the enzyme was maintained under reducing conditions and the nitrate concentration was stepwise increased, allowing the entire profile of i_{lim} against s to be recorded in seconds. The right panel shows the corresponding increase in activity against concentration which is fit to the Michaelis−Menten equation (eq 2a). The analysis of multiple runs gave $K_m^{lim} = 100 \pm 30\ \mu$M at pH 7 or 8, $T = 20$ °C. This is close to the value of the Michaelis constant measured in solution assays of the enzyme (170 μM in ref 26).

Modeling the Catalytic Wave Shapes for Nitrate Reduction. It may be unpractical to fit voltammetric data by adjusting the ten parameters in eq 2. In the case of NapAB, we could

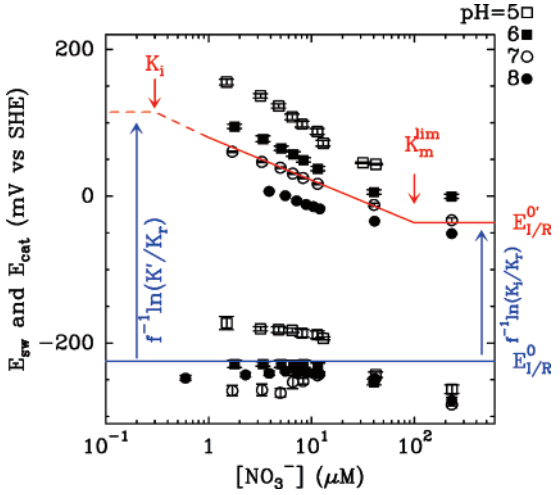

Figure 6. Dependence on substrate concentration of E_{cat} (top) and E_{sw} (bottom) at pH 5 (empty squares), 6 (filled squares), 7 (empty circles), and 8 (filled circles). Emphasis is on the low substrate concentration range ($s \ll K_m^{lim}$) which is best described by our model. The red line shows the dependence predicted by eq 3d. The exact value of K_i is unknown; only an upper limit can be estimated.

decrease the number of parameters by using an approximate rate equation which is given justification below.

Regarding the shape of the voltammograms for adsorbed NapAB, we observed that n_{sw} remains slightly smaller than 1 (typically between 0.8 and 1 under all conditions), while the low driving force part is essentially a one-electron wave (overall, it is slightly sharper at low s and broader at high s, and this is discussed below). Figure 6 shows how the positions of the inflection points of the voltammograms depend on substrate concentration and pH. We shall now interpret these values using the equations we derived for $E_{cat}^{n=1}$ and $E_{sw}^{n=1}$ (eqs 4d and 7b).

A first significant observation is that the position of the catalytic wave still shifts 60 mV per decade of s for $s < K_m^{lim}$, and there is no deviation from linearity even at the lowest accessible substrate concentrations. Using eq 3d, this implies $K_i \ll s \ll K'$. Second, from eq 8 and the fact that there is an extremum in the voltammogram in this range of concentration (hence $\alpha_i > \alpha_i^{min}$), we conclude that

$$\frac{k_i}{k_r} > 1 + \frac{k_{-r}}{k_2}\frac{s}{K_i} \qquad (9)$$

We now assume that k_i/k_r is not greater than a few units;[44] this will be checked *a posteriori* for consistency. Since $K_i \ll s$, eq 9 implies $k_{-r} \ll k_2$.

The same conclusion can be drawn from the following independent observation: Figure 6 shows that, in the range $K_i \ll s \ll K_m^{lim}$, E_1^{cat} is much greater than the reduction potential of the $Mo^{V/IV}$ couple ($E_{I/R}^{\circ} = -225$ mV at pH 7).[26] Since $E_{cat}^{n=1} - E_{I/R}^{\circ} \le f^{-1}\ln(K'/K_r)$ (Figure 4), we conclude that $K' \gg K_r$, hence $k_{-r} \ll k_2/\alpha_i$.

Besides, the condition $K_i \ll s$ implies $k_{-i} \ll k_i s$. Since both k_{-i} and k_{-r} are small, we shall proceed further by neglecting substrate release from the active site (we will check this below by letting on substrate release and observing no improvement of the model). Therefore, we consider a simplified version of the scheme in Figure 2 where all substrate-release steps are ignored. An additional simplification is that since $E_{O/I}^{\circ}$ is much greater than the range of electrode potential where catalysis is observed,[26] the steady-state concentration of species "O" is always very small and substrate binding to O does not occur.

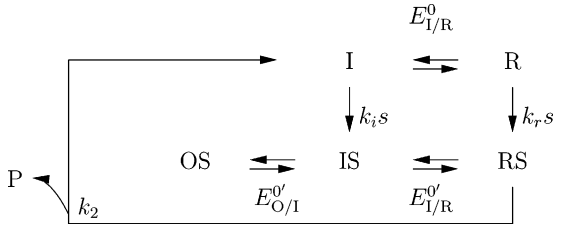

Figure 7. Simplified catalytic scheme for interpreting the voltammograms for adsorbed NapAB. This leads to the current eq 10.

This leads us to using the scheme shown in Figure 7 and the corresponding version of eq 2:

$$i_{\lim} = -\frac{2FA\Gamma k_2}{1 + K_m^{\lim}/s} \tag{10a}$$

$$K_m^{\lim} = \frac{k_2}{k_r} \tag{10b}$$

$$\frac{i_{\lim}}{i} = 1 + e'_{I/R}(1 + e'_{O/I}) + \frac{K_m^{\lim}}{s}\frac{1 + e_{I/R}}{1 + \alpha_i e_{I/R}} \tag{10c}$$

We used the compact notation $e_x = \exp[f(E - E_x^\circ)]$, $e'_x = \exp[f(E - E_x^{\circ\prime})]$. This equation predicts a main wave that can be broad ($n_{cat} = 1$ if $E^{\circ\prime}_{O/I} \gg E^{\circ\prime}_{I/R}$), sharp ($n_{cat} = 2$ if $E^{\circ\prime}_{O/I} \ll E^{\circ\prime}_{I/R}$), or nonsymmetrical in all other cases (sharper at the onset of activity than at lower potential if $E^{\circ\prime}_{O/I} \approx E^{\circ\prime}_{I/R}$). Indeed, the values of E_{cat} are given by

$$E_{cat}^{n=1} = E^{\circ\prime}_{I/R} + \frac{1}{f}\ln\left(1 + \frac{k_2}{k_i s}\right) \tag{11a}$$

$$E_{cat}^{n=2} = E^{\circ\prime}_{O/R} + \frac{1}{2f}\ln\left(1 + \frac{k_2}{k_i s}\right) \tag{11b}$$

If the low potential part of the wave shows a decrease in activity, then $n_{sw} = 1$ with

$$E_{sw}^{n=1} = E^\circ_{I/R} + \frac{1}{f}\ln\frac{1 + s\,k_t/k_2}{1 + s\,k_i/k_2} \tag{12}$$

The condition that a switch exists (formerly eq 8) now reads

$$k_i/k_r > 1 + \frac{s}{K_m^{\lim}}\exp[f(E^\circ_{I/R} - E^{\circ\prime}_{I/R})] \tag{13}$$

Figure 8 shows as red lines the best fits to eq 10c of catalytic voltammograms for NapAB in panels A and B and *E. coli* DMSO reductase (DmsABC) in panels C and D (the DmsABC data are from ref 25). Our goal here is to assess whether eq 10c can reproduce the *shape* of the voltammograms and not yet to interpret the values of the best parameters of the fit (this will occur later in this manuscript).

First, we note that in all cases the model can predict, at least roughly, the shapes and widths of the experimental wave shapes. Regarding the data recorded at low substrate concentration for NapAB (Figure 8A) and high pH for DmsABC (Figure 8C), the quality of the fits to eq 10 is remarkable. The insets are close-ups of the onset of activity. In addition to the same best fits shown as red curves, we plotted in blue the fits to eq 10 obtained by fixing $E^{\circ\prime}_{O/I}$ to a value arbitrarily large. These fits are significantly worse, demonstrating that the shape of the

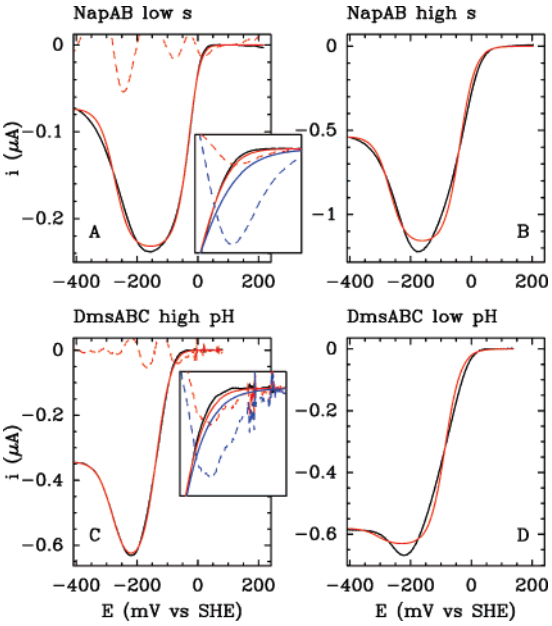

Figure 8. Activity against electrode potential for nitrate reduction by NapAB (top) or DMSO reduction by DmsABC (bottom). The red lines are best fits to eq 10c. The residuals enlarged 5 times are plotted as dashed lines. The insets show a close-up of the current at the onset of activity; therein, the blue lines are best fits to eq 10c with $E^{\circ\prime}_{O/I} \gg E^{\circ\prime}_{I/R}$. Top panels: NapAB, pH 8.5, $s = 7\ \mu$M (A) and $s = 40\ \mu$M (B). Bottom panels: DmsABC, $s = 20$ mM, pH 9 (C) and 6.5 (D). The data for DMSO reduction are those originally published in ref 25, redrawn and fit in panels C and D with permission from Prof. F. A. Armstrong, Oxford University.

voltammogram at high potential is best described if $E^{\circ\prime}_{O/I} \approx E^{\circ\prime}_{I/R}$. This is also observed for DmsABC in panel C.[45]

The fits in the left panels of Figure 8 demonstrate the very satisfactory agreement between the model and the data obtained for NapAB at low *s*. However, as shown in panel 8B, the wave predicted by eq 10 is significantly steeper than the experimental signal recorded at high concentration of nitrate and the same deviation is observed at low pH for DmsABC (panel 8D); this will be discussed later in this paper. Having shown that the scheme in Figure 7 can predict the shape of a voltammogram recorded under low substrate concentrations, we examine whether it can account for how the shape is modified upon changing the concentration of substrate for $s < 10\ \mu$M.

Data Analysis at Low Substrate Concentration. Six parameters may be adjusted to fit any voltammogram to eq 10: $E^\circ_{I/R}$, $E^{\circ\prime}_{I/R}$, $E^{\circ\prime}_{O/I}$, $2FA\Gamma k_2$, $K_m^{\lim}$, and α_i. We wonder whether they can be determined independently. In the limit of low *s* [strictly if $s \ll K_m^{\lim}$ and $s \ll K_m^{\lim}/\alpha_i$], eq 10 is well approximated by

$$\frac{2FA\Gamma k_2 s}{iK_m^{\lim}} \approx e'_{I/R}(1 + e'_{O/I}) + \frac{K_m^{\lim}}{s}\frac{1 + e_{I/R}}{1 + \alpha_i e_{I/R}} \tag{14}$$

Dividing both members of eq 14 by an arbitrary constant, *C*, we get

$$\frac{2FA\Gamma \tilde{k}_2 s}{iK_m^{\lim}} \approx \tilde{e}'_{I/R}(1 + e'_{O/I}) + \frac{\tilde{K}_m^{\lim}}{s}\frac{1 + e_{I/R}}{1 + \alpha_i e_{I/R}} \tag{15}$$

with $\tilde{k}_2 = k_2/C^2$, $\tilde{K}_m^{\lim} = K_m^{\lim}/C$, and $\tilde{E}^{\circ\prime}_{I/R} = E^{\circ\prime}_{I/R} + f^{-1}\ln(C)$. This demonstrates that if eq 10 is used to fit data recorded at low substrate concentration, the parameters $E^\circ_{I/R}$, $E^{\circ\prime}_{O/I}$, and α_i can be determined with no ambiguity. However, the best values of $2FA\Gamma k_2$, $E^{\circ\prime}_{I/R}$, and $K_m^{\lim}$ cannot be adjusted independently:

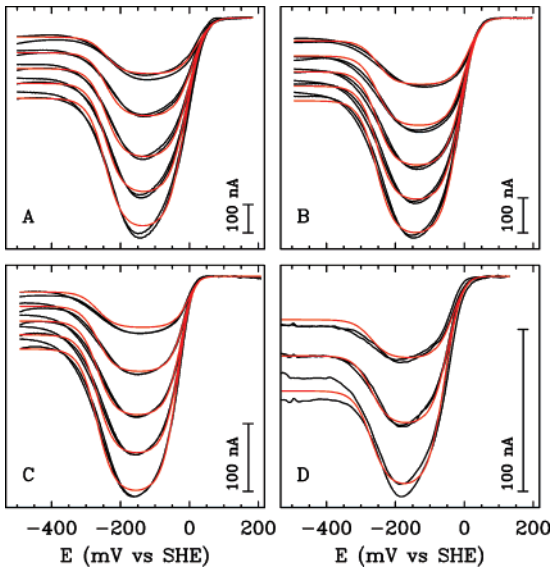

Figure 9. Baseline-subtracted voltammograms for nitrate reduction by adsorbed NapAB. The back lines come in pairs where each trace corresponds to data recorded by scanning the electrode potential in either direction. The red lines are best fits to eq 10 adjusting in each panel a single set of five independent parameters (see text). pH 7.5 (panel A, $s = 1.9$, 3.5, 5.2, 6.8, and 8.5 μM), pH 8 (panel B, $s = 2.3$, 3.9; 5.6, 7.2, and 8.9 μM), pH 8.4 (C, $s = 1.7$, 3.3, 5, 6.6, and 8.2 μM), and pH 9 (D, $s = 3.8$, 7.1, and 10.4 μM). $\nu = 20$ mV/s, $T = 20$ °C, $\omega = 2.3$ krpm.

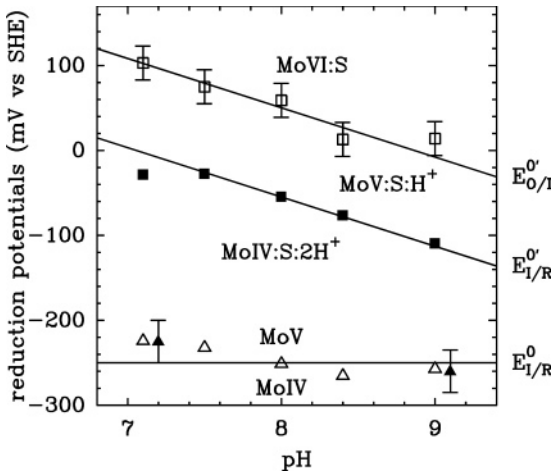

Figure 10. Pourbaix diagram showing the pH dependences of the reduction potentials determined from fitting the data in Figure 9 to eq 10: $E^{\circ}_{I/R}$ (triangles); $E^{\circ\prime}_{I/R}$ (closed squares); $E^{\circ\prime}_{O/I}$ (open squares). The straight lines have a slope of zero or $-2.3RT/F$; the latter reveals a one-electron reduction that is coupled to the uptake of one proton. The filled triangles show the values measured in potentiometric titrations of the active site followed by EPR.

fitting the data by adjusting only five parameters and fixing, for example, K_m^{lim} to a value C times smaller than the real value would return the same fit as with six adjustable parameters, but Γk_2 would be underestimated by a factor of C^2 and $E^{\circ\prime}_{I/R}$ would be $f^{-1}\ln(C)$ too high.[46]

Therefore, we fit the changes in activity against E and s to eq 10, adjusting five *independent* parameters, $E^{\circ}_{I/R}$, $E^{\circ\prime}_{I/R}$, $E^{\circ\prime}_{O/I}$, α_i, and $2FA\Gamma k_2$, after having fixed K_m^{lim} to a value which we independently determined. From chronoamperometric experiments such as those in Figure 5, we measured the following: $K_m^{lim} = 100 \pm 30$ μM at pH 7−8, 140 ± 30 μM at pH 8.4, and 185 ± 30 μM at pH 9.[47]

In Figure 9, the four panels show data recorded at four different pH values and up to five different concentrations of nitrate (from 1.5 to 9 μM). For each set of experimental conditions, two black lines correspond to the baseline-subtracted voltammograms recorded by scanning the electrode potential upward or downward; the very satisfactory overlay proves that the scan rate was low enough that steady state was achieved. The best fits are shown as red lines; it is fairly obvious that, in this range of experimental conditions, eq 10 reproduces very accurately both the wave shape and the way the shapes change as the concentration of substrate is raised.

Figure 10 shows how the adjusted values of the reduction potentials depend on pH. The values of $E^{\circ}_{I/R}$ (the reduction potential of the $Mo^{V/IV}$ couple) show little pH dependence and match very accurately those independently measured in potentiometric titrations of the EPR Mo^{V} signal (black triangles).[26] The two reduction potentials of the substrate-bound Mo couples decrease 60 mV per pH unit, as expected for one-electron/one-proton reductions. The value of $\alpha_i = k_i/k_r$ determined from fitting the data in Figure 9 equates to 3 ± 1, showing that even a slightly faster binding to Mo^{V} than to Mo^{IV} has a strong impact on the shape of the catalytic signal, provided the condition given by eq 13 holds. The exponential term in eq 13 is very small; this explains that the switch is still observed at substrate concentrations much greater than K_m^{lim} (Figure 1).

Allowing Substrate Release Does Not Improve the Fits. We have greatly simplified the scheme in Figure 2 and the corresponding rate equation to decrease from 10 to 5 the number of parameters that must be adjusted to fit the data in Figure 9. Although our assumptions were given justification, we found it useful to check *a posteriori* that the fits we obtained were unique by allowing substrate release from R and I in the scheme in Figure 7. We repeated the fits adjusting two additional parameters accounting for substrate release, k_{-r}/k_2 and k_{-i}/k_2. In all cases, the best values of the other five parameters were not significantly changed, while the best values of k_{-r}/k_2 and k_{-i}/k_2 were found to be smaller than 10^{-1} in the worst case and often much smaller. In particular, k_{-r}/k_2 must be extremely small in order to reproduce the change in E_{cat} against s.

Departure from the Predictions of the Scheme in Figure 2 at High Substrate Concentrations. The right panels in Figure 8 show that the theoretical waves predicted by eq 10 are significantly steeper than those observed at high s.

Our assumptions that voltammetry is at steady state and that there is no limitation by mass transport cannot explain the discrepancy between the prediction of the scheme in Figure 2 and the data: stationarity was confirmed by the fact that the wave shape is independent of scan direction (Figure 9), and the condition that there is no mass transport control is even less restrictive at high substrate concentration than for $s \ll K_m^{lim}$. Regarding our assumption of fast electron transfer, it may be thought that the difference between the model and the data arises from interfacial ET (between the electrode and the enzyme) becoming rate limiting when the enzyme turnover increases: indeed, the prediction of previously proposed models that do not assume fast interfacial ET[3,5,7,48] is that if interfacial ET is not very fast with respect to turnover rate, the apparent n value may be either 1 or 2 at the onset of activity and then decrease to $^1/_2$ before the maximal current is reached, giving rise to an asymmetrical wave that broadens as the driving force increases.[49] Although this seems consistent with the change in shape seen in Figure 1 as the current increases, the experiments we discuss below challenge this explanation.

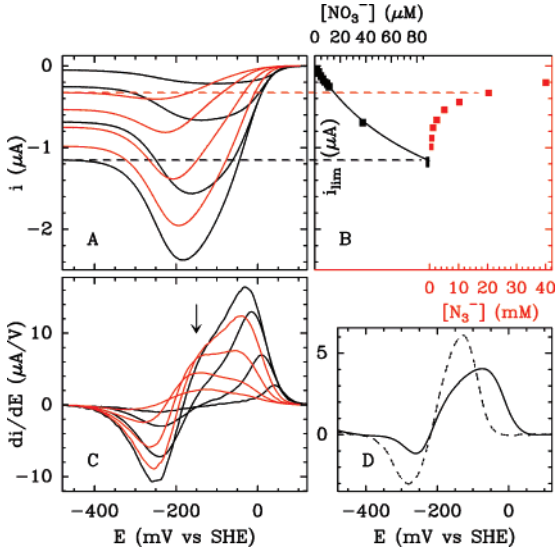

Figure 11. (A) The black lines are catalytic signals for nitrate reduction at pH 7.5, $s = 1.5-40$ μM. The red lines show how the signal is modified upon adding azide in concentration 0.3−40 mM. The concentrations and limiting currents are indicated in panel B, and panel C shows the first derivatives of these data. Panel D shows the derivatives of the data for DMSO reduction by DmsABC[25] shown in Figure 8D; pH 9 (solid line) and pH 7 (dashed line) (with permission).

Figure 11C shows the first derivative of catalytic voltammograms in panel A, recorded at pH 7 for increasing concentrations of nitrate. The broadening of the wave is seen as an increase in the width of the positive peak upon increasing substrate concentration, and as a shoulder on the left flank of the peak (marked by an arrow at $E \approx -150$ mV). The same effect can be obtained when the competitive inhibitor[50,51] azide is added, as shown by the red lines in Figure 11. The magnitude of the current decreases upon increasing the concentration of azide (and so does the magnitude of the first derivative), but the shape of the voltammogram is also modified: the main wave significantly broadens and a second component grows under the high potential peak in the derivative of the data, matching the shoulder seen at −150 mV in the absence of inhibitor. Since the inhibitor decreases the turnover rate, this demonstrates that the broadening does not result from interfacial ET becoming rate limiting. Instead, this suggests that, in the absence of inhibitor and at high s, a sigmoidal component at −150 mV takes over the main wave at about 0 mV. Importantly, a similar broadening is also seen in the derivative of the voltammograms for DMSO reduction by DmsABC in panel D, revealing common kinetic properties in enzymes from the DMSO reductase family.

Such a complex feature in the voltammogram is likely to reveal the existence of chemical steps whose rates are large enough so as to become rate limiting only at high substrate concentration, when the turnover rate is high (hence these steps do not affect the signal at low substrate concentration). We are in the process of complexifying the scheme in Figure 2 in order to account for the peculiar shape of the voltammograms recorded under these conditions. This is out of the scope of this paper.

Discussion

Interpreting the Catalytic Potential and the Appearance of Complex Voltammetric Features. Substrate binding to multiple redox states of the active site needs to be taken into account for interpreting the voltammetry of adsorbed enzymes, whatever shape the wave takes, but most electrochemical models have assumed that substrate binds only when the active site is in the redox state that is competent to turn it over.[3,14−17] In contrast, for interpreting the apparently simple voltammetric response for NiFe hydrogenase and fumarate reductase, the following strategy made it possible to model the data by *allowing* substrate (proton or succinate) binding to any redox state of the active site without adding parameters that would have been difficult to determine unambiguously.[6,7] The voltammograms recorded for various concentrations of substrate were fit to a generic equation like

$$i = \frac{i_{\lim}}{1 + \exp[f(E - E^0_{I/R})] + \exp[2f(E - E^0_{O/R})]} \quad (16)$$

by adjusting at each concentration the limiting current and the two reduction potentials of the active site $E^0_{I/R}$ and $E^0_{O/R}$. In a second step, the dependence of these parameters on substrate concentration and pH was plotted in a Pourbaix diagram of $E°$ against pH or log(s) to determine the values of the pK_a and substrate dissociation constants of the active site in each of its redox states. For hydrogenase, the emerging picture was that when the enzyme produces hydrogen, each electron transfer to the active site is followed by one protonation,[7] whereas the oxidation state of the active site flavin of fumarate reductase has little influence on its affinity for succinate.[6] In this approach, it is expected that, in the limit of low substrate concentration, the reduction potential measured from the position of the wave tends to the value that can be determined in potentiometric titrations (which are necessarily carried out in the absence of substrate). For various enzymes, this principle helped the qualitative interpretation of the position of the main wave,[15,24,34] and the departure from this expected behavior has been discussed in relation to the mechanism on a case-by-case basis.[15,34]

However, the major assumption that protonation and substrate binding are at equilibrium in the steady state may be difficult to check *a posteriori* and it may be feared that the interpretation of the substrate concentration dependence of the position of the wave and of the value it takes at low substrate concentration are incorrectly interpreted if theses processes are slow on the time scale of turnover. This important point is examined in the model we propose, which explicitly takes into account substrate binding and release to any redox state of the active site (binding to a single state may be considered as a peculiar case) but makes no assumption about the kinetics of this process. The rate equations could be factorized into simple expressions embedding a small number of *apparent* parameters, which can be discussed and easily determined from fitting the data.

Regarding the position of the main wave (the value of E_{cat}), we examined a first limiting situation where substrate binding and release are fast with respect to turnover ($k_2 \rightarrow 0$). In this case, the position of the catalytic wave, E_{cat}, continuously drifts from the substrate-free to the substrate-bound value of the reduction potential of the active site upon increasing substrate concentration, and is as predicted by thermodynamics (eq 5): it can be plotted in a Pourbaix-like diagram (solid lines in Figure 4) to measure the dissociation constants from the active site, the effect of substrate binding on the active site reduction potential, and particularly the value of the latter in the absence of substrate by extrapolating to zero concentration.

However, we showed that if substrate binding is not at equilibrium in the steady state, the dependence of the apparent reduction potential of the active site on substrate concentration takes the same form as that predicted for fast binding, but this

TABLE 1: Equilibrium and Catalytic Redox Properties of Enzymes from the DMSO Reductase Family[a]

organism	enzyme	pH	E_{cat}	E_{sw}	$E°(Mo^{V/IV})$	$E°(Mo^{VI/V})$	reference
R. sphaeroides	NapAB	7	$\approx +50$	≈ -250	-225	$+550$	this work and ref 26
S. elongatus	NarB	8	-300	-500	< -550	-150	33
E. coli	DmsABC	9	-140	-280	-230	-83	25
P. pantotrophus	NarGH	6	$+90$	-30	-50	$+470$	18

[a] In all cases, the catalytic waves are centered on a potential of $E_{cat} \gg E°(Mo^{V/IV})$, while the potential of the switch correlates more closely with $E°(Mo^{V/IV})$, as predicted by our model (eqs 11a and 12). Potentials are in units of mV vs SHE. $E°(Mo^{V/IV})$ and $E°(Mo^{VI/V})$ are the reduction potentials of the Mo couples.

is misleading because the inflection points in the Pourbaix diagram of E_{cat} against log(s) can no longer be interpreted as being true dissociation constants, and the position of the wave in the limit of low s no longer tends to the reduction potential of the active site free of substrate (dashed lines in Figure 4). NapAB illustrates an extreme situation where substrate binding is fully irreversible on the time scale of turnover; in that case, the position of the catalytic wave (that is the apparent reduction potential of the active site) is close to the reduction potential of the substrate-bound Mo *even at the lowest substrate concentrations* (eq 11a and Figure 6).

Besides providing a framework in which one can interpret the position of the main wave, the model which considers differential binding predicts that the wave can take the various shapes shown in Figure 3. It is striking that all of them have been observed for various systems[6,11,25,34] (of course, we do not mean to imply that the model we propose will apply in all cases). Regarding catalytic waves showing an extremum in activity when the electrode potential is varied, the analogy between the activity of a redox enzyme being optimized over a certain potential range and the usual bell-shaped curves of activity against pH has already be noted:[4,25] just as maximal activity commonly requires that the pH not be extreme, important (or faster) steps in the catalytic cycle of a redox enzyme may occur when the active site is in an intermediate redox state. This is allowed by the scheme in Figure 2 according to which the sequence of events in the catalytic cycle depends on the driving force, and consequently, the turnover rate need not vary in a monotonous fashion with the electrode potential. According to this scheme, the voltammogram should tend to a simpler form as the substrate concentration is raised because the substrate binding steps no longer limit catalysis. Importantly, the possibility that differential binding is the reason the wave is not sigmoidal cannot be excluded on the basis that the switch remains visible under saturating conditions:[20,21] the simple criterion in eq 8 demonstrates that the substrate concentration that is high enough that the switch disappears is not simply related to, and can be much greater than K_m. This may be so, for example, in cases where substrate binding is irreversible.

The Reductive Half-Cycle in NapAB. In the case of NapAB and other enzymes from the DMSO reductase family, not only is the shape of the voltammogram complex, but also its position along the E axis used to make little sense. Indeed, since formation of nitrite requires that the active site is reduced to Mo^{IV}, one may expect the activity to appear when the electrode potential is taken below the reduction potential of the $Mo^{V/IV}$ couple (-225 mV vs SHE at pH 7). Instead, catalysis by NapAB kicks on at an electrode potential that is well above the reduction potential of $Mo^{V/IV}$ and the activity drops off dramatically when the reduction potential of $Mo^{V/IV}$ is reached (Figure 1). This counterintuitive behavior is observed for other enzymes from the DMSO reductase family for which PFV data are available (Table 1), suggesting a common origin in terms of catalytic mechanism. This is simply explained by the model we propose.

The catalytic cycle of nitrate reductase can be split into two halves. In the reductive part, two electron transfers from the redox partner (here the electrode) to the oxidized Mo^{VI}-oxo active site reduce it to the +IV state, which is catalytically competent to reduce nitrate. In the oxidative half-cycle, the Mo^{VI} state is regenerated upon nitrite formation. The rate of the latter reaction, k_2, mainly affects the magnitude of the electrochemical data, whereas the voltammetric wave shapes contain detailed information about the reductive half-cycle, particularly the succession of chemical reactions that are coupled to electron transfer (ET) and lead to the formation of the substrate-bound, fully reduced species.

Using the general predictions of the six-member scheme in Figure 2, we conclude that nitrate binding is essentially irreversible. This led us to using the simplified scheme in Figure 7 and the steady-state rate equation (eq 10) that could be used to interpret the data over a range of experimental parameters where perfect agreement was found, that is, the entire range of driving force, pH neutral or alkaline, and low (and physiological) substrate concentration (Figure 9). We discussed the possible reasons deviations are observed under certain experimental conditions. In fitting the data, we also took great care regarding which of the parameters in the model could be determined independently. This led us to an unambiguous description of the catalytic cycle.

Chemical Events (Including Protonations) Coupled to ET to the Active Site. Our strategy to interpret the data consisted of two steps. First, we used a model where protonation steps are not explicit (scheme in Figure 7 and eq 10) to fit electrochemical data recorded at different pH values (Figure 9) and we determined the pH-dependent reduction potentials of the intermediates. In a second step, the pH dependences in Figure 10 can be interpreted to detect redox-coupled protonations and to deduce the entire sequence of events that take place during the reductive catalytic half-cycle. The emerging picture is that, at moderate driving force, substrate binds to Mo^{V} and the resulting complex takes up one proton. The second protonation occurs only after a second electron transfer from the proximal $[4Fe4S]^{+}$ cluster further reduces the substrate-bound active site to Mo^{IV}, yielding the species that is competent to produce nitrite. The protonation step may be the main reason the reduction potential of the substrate-bound $Mo^{V/IV}$ couple is significantly raised upon substrate binding.

Irreversible Chemical Steps and the Thermodynamics of Intramolecular Electron Transfer. In the reductive half-cycle of NapAB, Mo^{VI} is reduced to Mo^{V} upon electron transfer from the proximal $[4Fe4S]^{+}$ cluster in a thermodynamically favorable step ($E°(Mo^{VI/V}) \approx +550$ mV, $E°([4Fe4S]^{2+/+} = -80$ mV). Should a second electron-transfer step from $[4Fe4S]^{+}$ to Mo^{V} occur, this step would be endergonic ($E°(Mo^{V/IV}) = -225$ mV). However, the conclusion from the electrochemical study is that the formation of Mo^{V} is followed by substrate binding and protonation, and this results in a large increase in the reduction potential of $Mo^{V/IV}$ (ca 200 mV, Figure 10). This decreases the driving force that is required to fully reduce the Moco, and the

reduction potential of the [4Fe4S] cluster is low enough that electrons can be transferred to substrate-bound Mo^V in an exergonic step. This illustrates a situation where the value of the reduction potential of the substrate-free $Mo^{V/IV}$ couple which is obtained from equilibrium titrations is not relevant to describe the thermodynamics of electron transfer during the catalytic cycle.

There are several cases in the literature of substrate binding having a strong effect on the reduction potential of the active site in a way that favors inter- or intramolecular electron transfer. This occurs, for example, in cytochromes P450[52,53] and copper-containing nitrite reductase.[54] In a system related to ours, xanthine oxidase, binding of the substrate analogue 8-bromo-xanthine increases the reduction potential of the $Mo^{V/IV}$ couple,[55] but this is believed to be the reason enzyme activity drops off dramatically at high substrate concentration, as substrate binding increases the level of reduced enzyme in the steady state.

Such effects are always difficult to detect in potentiometric experiments because it is usually not possible to titrate the active site in the presence of substrate without the enzyme turning over (inhibitors are sometimes used to probe enzyme−substrate interactions). In terms of thermodynamics, the greater affinity of substrate for a certain redox state of the active site affects the reduction potential of the active site *bound to substrate*. Whether the active site is saturated with substrate in the steady state should be determined by comparing the physiological substrate concentration and the values of the equilibrium dissociation constants.

Direct electrochemistry makes it possible to probe the redox properties of the active site under turnover conditions, and the model we propose adds the kinetic dimension to the above discussion: for given concentration and dissociation constants, the kinetics of substrate binding may affect the fraction of active site that is bound to substrate in the steady state. If substrate binding and release is fast with respect to turnover ($k_2 \rightarrow 0$), the effect of substrate binding occurs only at high substrate concentration, when the active sites are mostly bound to substrate in the steady state. NapAB illustrates the opposite limiting case where substrate binding is irreversible on the time scale of turnover. In this situation, the effect of substrate binding on the energetics of intramolecular ET results from the concerted effects of thermodynamics (substrate binding and protonations raising the reduction potential of the $Mo^{V/IV}$ couple) and kinetics (the irreversibility of the chemical steps triggered by substrate binding making this happen even at concentrations of nitrate well below saturation).

The fact that nitrate binding in NapAB is irreversible may also be one of the reasons this enzyme, unlike nitrite oxidases from *Nitrobacter* species[56,57] which also belong to the DMSO reductase family, has no detectable oxidative activity: catalytic nitrite oxidation would necessarily involve a step of nitrate release from the active site.

Acknowledgment. We are grateful to Jérôme Lavergne (CEA Cadarache) for his comments on the manuscript. This work was funded by the French CNRS, CEA and ANR (PCV program 2006-2009), the University of Provence, and the City of Marseilles.

Supporting Information Available: A complete list of symbols, the derivations of eqs 2−4, 6, and 7, and the parameters used to calculate the voltammograms in Figure 3. This material is available free of charge via the Internet at http://pubs.acs.org.

References and Notes

(1) Léger, C.; Elliott, S. J.; Hoke, K. R.; Jeuken, L. J. C.; Jones, A. K.; Armstrong, F. A. *Biochemistry* **2003**, *42*, 8653−8662 (http://dx.doi.org/10.1021/bi034789c).

(2) Armstrong, F. A. *Curr. Opin. Chem. Biol.* **2005**, *9*, 110−117 (http://dx.doi.org/10.1016/j.cbpa.2005.02.011).

(3) Heering, H. A.; Hirst, J.; Armstrong, F. A. *J. Phys. Chem. B* **1998**, *102*, 6889−6902 (http://dx.doi.org/10.1021/jp981023r).

(4) Elliott, S. J.; Léger, C.; Pershad, H. R.; Hirst, J.; Heffron, K.; Blasco, F.; Rothery, R.; Weiner, J.; Armstrong, F. A. *Biochim. Biophys. Acta* **2002**, 1555, 54−59 (http://dx.doi.org/10.1016/S0005−2728(02)00254−2).

(5) Léger, C.; Lederer, F.; Guigliarelli, B.; Pertrand, P. *J. Am. Chem. Soc.* **2006**, *128*, 180−187 (http://dx.doi.org/10.1021/ja055275z).

(6) Léger, C.; Heffron, K.; Pershad, H. R.; Maklashina, E.; Luna-Chavez, C.; Cecchini, G.; Ackrell, B. A. C.; Armstrong, F. A. *Biochemistry* **2001**, *40*, 11234−11245 (http://dx.doi.org/10.1021/bi010889b).

(7) Léger, C.; Jones, A. K.; Roseboom, W.; Albracht, S. P. J.; Armstrong, F. A. *Biochemistry* **2002**, *41*, 15736−15746 (http://dx.doi.org/10.1021/bi026586e).

(8) Stankovich, M. T. Redox properties of flavins and flavoproteins. In *Chemistry and Biochemistry of flavoenzymes*, Vol. 1; Franz Müller, P., Ed.; CRC Press, Inc: Boca Raton, FL, Ann Arbor, MI, Boston, MA, London, 1991.

(9) Sucheta, A.; Cammack, R.; Weiner, J.; Armstrong, F. A. *Biochemistry* **1993**, *32*, 5455−5465 (http://dx.doi.org/10.1021/bi00071a023).

(10) Heering, H. A.; Weiner, J. H.; Armstrong, F. A. *J. Am. Chem. Soc.* **1997**, *119*, 11628−11638 (http://dx.doi.org/10.1021/ja9723242).

(11) Hudson, J. M.; Heffron, K.; Kotlyar, V.; Sher, Y.; Maklashina, E.; Cecchini, G.; Armstrong, F. A. *J. Am. Chem. Soc.* **2005**, *127*, 6977−6989 (http://dx.doi.org/10.1021/ja043404q).

(12) Sucheta, A.; Ackrell, B. A. C.; Cochran, B.; Armstrong, F. A. *Nature* **1992**, *356*, 361−362 (http://dx.doi.org/10.1038/356361a0).

(13) Ackrell, B. A. C.; Armstrong, F. A.; Cochran, B.; Sucheta, A.; Yu, T. *FEBS Lett.* **1993**, *326*, 92−94 (http://dx.doi.org/10.1016/0014−5793-(93)81768-U).

(14) Reda, T.; Hirst, J. *J. Phys. Chem. B* **2006**, *10*, 1394−1404 (http://dx.doi.org/10.1021/jp054783s).

(15) Barker, C.; Reda, T.; Hirst, J. *Biochemistry* **2007**, *46*, 3454−3464 (http://dx.doi.org/10.1021/bi061988y).

(16) Honeychurch, M. J.; Bernhardt, P. V. *J. Phys. Chem. B* **2005**, *109*, 5766−5773 (http://dx.doi.org/10.1021/jp0454570).

(17) Andreu, R.; Ferapontova, E.; Gorton, L.; Calvente, J. *J. Phys. Chem. B* **2007**, *111*, 469−477 (http://dx.doi.org/10.1021/jp064277i).

(18) Anderson, L. J.; Richardson, D. J.; Butt, J. N. *Biochemistry* **2001**, *40*, 11294−11307 (http://dx.doi.org/10.1021/bi002706b).

(19) Frangioni, B.; Arnoux, P.; Sabaty, M.; Pignol, D.; Bertrand, P.; Guigliarelli, B.; Léger, C. *J. Am. Chem. Soc.* **2004**, *126*, 1328−1329 (http://dx.doi.org/10.1021/ja0384072).

(20) Hirst, J.; Sucheta, A.; Ackrell, B. A. C.; Armstrong, F. A. *J. Am. Chem. Soc.* **1996**, *118*, 5031−5038 (http://dx.doi.org/10.1021/ja9534361).

(21) Hirst, J.; Ackrell, B. A. C.; Armstrong, F. A. *J. Am. Chem. Soc.* **1997**, *119*, 7434−7439 (http://dx.doi.org/10.1021/ja9631413).

(22) Pershad, H. R.; Hirst, J.; Cochran, B.; Ackrell, B. A. C.; Armstrong, F. A. *Biochim. Biophys. Acta* **1999**, *1412*, 262−272 (http://dx.doi.org/10.1016/S0005−2728(99)00066−3).

(23) Angove, H. C.; Cole, J. A.; Richardson, D. J.; Butt, J. N. *J. Biol. Chem.* **2002**, *277*, 23374−23381 (http://dx.doi.org/10.1074/jbc.M200495200).

(24) Gwyer, J. D.; Richardson, D. J.; Butt, J. N. *J. Am. Chem. Soc.* **2005**, *127*, 14964−14965 (http://dx.doi.org/10.1021/ja054160s).

(25) Heffron, K.; Léger, C.; Rothery, R. A.; Weiner, J. H.; Armstrong, F. A. *Biochemistry* **2001**, *40*, 3117−3126 (http://dx.doi.org/10.1021/bi002452u).

(26) Arnoux, P.; Sabaty, M.; Alric, J.; Frangioni, B.; Guigliarelli, B.; Adriano, J. M.; Pignol, D. *Nat. Struct. Biol.* **2003**, *10*, 928−934 (http://dx.doi.org/10.1038/nsb994).

(27) Moura, J. J.; Brondino, C. D.; Trincao, J.; Romao, M. J. *J. Biol. Inorg. Chem.* **2004**, *9*, 791−799 (http://dx.doi.org/10.1007/s00775−004-0573−9).

(28) Jormakka, M.; Tornroth, S.; Byrne, B.; Iwata, S. *Science* **2002**, *295*, 1863−1868 (http://dx.doi.org/10.1126/science.1068186).

(29) Bertero, M. G.; Rothery, R. A.; Palak, M.; Hou, C.; Lim, D.; Blasco, F.; Weiner, J. H.; Strynadka, N. C. J. *Nat. Struct. Biol.* **2003**, *10*, 681−687 (http://dx.doi.org/10.1038/nsb969).

(30) Lanciano, P.; Magalon, A.; Bertrand, P.; Guigliarelli, B.; Grimaldi, S. *Biochemistry* **2007**, *46*, 5323−5329 (http://dx.doi.org/10.1021/bi700074y).

(31) Ellis, P. J.; Conrads, T.; Hille, R.; Kuhn, P. *Structure* **2001**, *9*, 125−132 (http://Dx.doi.org/10.1016/S0969-2126(01)00566-4).

(32) Sabaty, M.; Avazeri, C.; Pignol, D.; Vermeglio, A. *Appl. Environ. Microbiol.* **2001**, *67*, 5122−5126 (http://dx.doi.org/10.1128/AEM.67.11.5122-5126.2001).

(33) Jepson, B. J. N.; Anderson, L. J.; Rubio, L. M.; Taylor, C. J.; Butler, C. S.; Flores, E.; Herrero, A.; Butt, J. N.; Richardson, D. J. *J. Biol. Chem.* **2004**, *279*, 32212−32218 (http://dx.doi.org/10.1074/jbc.M402669200).

(34) Elliott, S. J.; Hoke, K. R.; Heffron, K.; Rothery, R. A.; Weiner, J. H.; Armstrong, F. A. *Biochemistry* **2004**, *43*, 799−807 (http://dx.doi.org/10.1021/bi035869j).

(35) Hoke, K. R.; Cobb, N.; Armstrong, F. A.; Hille, R. *Biochemistry* **2004**, *43*, 1667−1674 (http://dx.doi.org/10.1021/bi0357154).

(36) Bernhardt, P. V.; Santini, J. M. *Biochemistry* **2006**, *45*, 2804−2809 (http://dx.doi.org/10.1021/bi0522448).

(37) Léger, C.; Dementin, S.; Bertrand, P.; Rousset, M.; Guigliarelli, B. *J. Am. Chem. Soc.* **2004**, *126*, 12162−12172 (http://dx.doi.org/10.1021/ja046548d).

(38) Boggs, P. T.; Donaldson, J. R.; Byrd, R. H.; Schnabel, R. B. *ACM Trans. Math. Software* **1989**, *15*, 348−364 (http://doi.acm.org/10.1145/76909.76913).

(39) Zu, Y.; Shannon, R. J.; Hirst, J. *J. Am. Chem. Soc.* **2003**, *125*, 6020−6021 (http://dx.doi.org/10.1021/ja0343961).

(40) Cornish-Bowden, A. *Fundamentals of Enzyme kinetics*; Portland Press: London, 2004.

(41) Martínez-Espinosa, R. M.; Richardson, D. J. J. B.; Bonete, M. *Biochem. Soc. Trans.* **2005**, *34*, 115−117.

(42) Field, S. J.; Thornton, N. P.; Anderson, L. J.; Gates, A. J.; Reilly, A.; Jepson, B. J. N.; Richardson, D. J.; George, S. J.; Cheesmana, M. R.; Butt, J. N. *Dalton Trans.* **2005**, 3580−3586 (http://dx.doi.org/10.1039/b505530j).

(43) Almeida, M. G.; Guigliarelli, B.; Bertrand, P.; Moura, J. J. G.; Moura, I.; Léger, C. *FEBS Lett.* **2007**, *581*, 284−288 (http://dx.doi.org/10.1016/j.febslet.2006.12.023).

(44) We know that $k_i/k_r \geq i_{peak}/i_{lim}$ if substrate binding is irreversible.[19]

(45) The deviation from $n_{cat} = 1$ at the onset of activity is also apparent in Figure 6 of ref 25.

(46) This is equivalent to a situation in solution assays where the slope of the linear change in activity against s at $s \ll K_m^{lim}$ can be used to determine only the second-order rate constant, k_{cat}/K_m^{lim}, but not k_{cat} and K_m^{lim} independently.

(47) When the value of K_m^{lim} is fixed in the fitting procedure, the above analysis shows that an error, ΔK_m, on K_m^{lim} results in an error on $E^{\circ\prime}_{I/R}$ that equates $f^{-1} \ln(1 + (\Delta K_m^{lim}/K_m^{lim}))$, that is only a few mV even if ΔK_m^{lim} is large ($\Delta E^{\circ\prime}_{I/R} < 7$mV for $\Delta K_m^{lim}/K_m^{lim} = 30\%$).

(48) Léger, C.; Jones, A. K.; Albracht, S. P. J.; Armstrong., F. A. *J. Phys. Chem. B* **2002**, *106*, 13058−13063 (http://dx.doi.org/10.1021/jp0265687).

(49) The limit $n = {}^1/_2$ is that predicted if the Butler−Volmer theory of ET is used (ref 3 and the Appendix of ref 48). If the interfacial ET is described by Marcus theory, the wave can broaden even more.[3]

(50) Butler, C.; Charnock, J.; Bennett, B.; Sears, H.; Reilly, A.; Ferguson, S.; Garner, C.; Lowe, D.; Thomson, A.; Berks, B.; Richardson, D. *Biochemistry* **1999**, *38*, 9000−9012 (http://dx.doi.org/10.1021/bi990402n).

(51) Butler, C. S.; Fairhurst, S. A.; Ferguson, S. J.; Thomson, A. J.; Berks, B. C.; Richardson, D. J.; Lowe, D. J. *Biochem. J.* **2002**, *363*, 817−823 (http://www.biochemj.org/bj/363/bj3630817.htm).

(52) Sharp, R. E.; Chapman, S. K. *Biochim. Biophys. Acta* **1999**, *1432*, 143−158 (http://dx.doi.org/10.1016/S0167-4838(99)00109-0).

(53) Daff, S. N.; Chapman, S. K.; Turner, K. L.; Holt, R. A.; Govindaraj, S.; Poulos, T. L.; Munro, A. W. *Biochemistry* **1997**, *36*, 13816−13823 (http://dx.doi.org/10.1021/bi971085s).

(54) Pinho, D.; Besson, S.; Brondino, C. D.; de Castro, B.; Moura, I. *Eur. J. Biochem.* **2004**, *271*, 2361−2369 (http://dx.doi.org/10.1111/j.1432-1033.2004.04155.x).

(55) Hille, R.; Stewart, R. C. *J. Biol. Chem.* **1984**, *259*, 1570−1576 (http://www.jbc.org/cgi/content/abstract/259/3/1570).

(56) Meincke, M.; Bock, E.; Kastrau, D.; Kroneck, P. M. H. *Arch. Microbiol.* **1992**, *158*, 127−131 (http://dx.doi.org/10.1007/BF00245215).

(57) Starkenburg, S. R.; Chain, P. S. G.; Sayavedra-Soto, L. A.; Hauser, L.; Land, M. L.; Larimer, F. W.; Malfatti, S. A.; Klotz, M. G.; Bottomley, P. J.; Arp, D. J.; Hicke, W. J. *Appl. Environ. Microbiol.* **2006**, *72*, 2050−2063 (http://dx.doi.org/10.1128/AEM.72.3.2050-2063.2006).